Distributed neurodynamic algorithms for collaborative energy management in energy internet considering time-varying factors ☆

Gui Zhao [a], Xing He [a,*], Guo Chen [b], Chaojie Li [c]

[a] *Chongqing Key Laboratory of Nonlinear Circuits and Intelligent Information Processing, College of Electronic and Information Engineering, Southwest University, Chongqing, 400715, China*
[b] *The School of Electrical Engineering and Computer Science, University of Newcastle, Newcastle, NSW 2308, Australia*
[c] *The School of Electrical Engineering and Telecommunications, The University of New South Wales, Sydney, NSW 2052, Australia*

ARTICLE INFO

ABSTRACT

This paper investigates the energy management problem of the energy Internet under time-varying conditions . In the context of coupled multi-energy networks, the energy Internet is considered to be composed of multiple energy bodies and requires collaborative planning of multiple energy networks. A model for distributed energy management with a non-smooth cost function and line congestion constraints is proposed, with the goal of reducing overall operating costs and improving customer benefits while considering load as a time-varying factor. Then, a neurodynamic time-varying algorithm for addressing the energy management problem executed in a fully distributed manner is proposed. On the one hand, the predictive effect of the differential feedback term is exploited and embedded in the implementation of the proposed algorithm, thus speeding up the convergence. On the other hand, the algorithm is executed in a distributed manner, and only limited information is exchanged among the agents to complete the optimal operation locally, thus reducing the communication burden and ensuring privacy and robustness. Finally, theoretical proofs guarantee the stability of the proposed algorithm, and simulation experiments illustrate the effectiveness and robustness of the proposed algorithm.

1. Introduction

Increasing environmental pollution and energy crisis have placed higher demands on current energy systems [1]. For this reason, it is imperative to conduct research on multi-energy systems. Research for multi-energy systems has been dedicated to making full use of the mutual aid and complementarity of different forms of energy, improving system economy, enhancing system flexibility and increasing system reliability [2,3]. In recent years, the concept of Energy Internet (EI) has emerged, based on the multi-energy system (MES), using advanced power electronics, information technology and intelligent management technology, interconnecting energy networks such as smart grid (SG), heating network and gas supply network to achieve energy and information sharing, which is considered as a clean and efficient future energy system [4–6].

As a component of EI, the SG has been a hot research topic in recent years, in which a great deal of research work has been carried out by scholars related to the voltage optimization problem (VOP)

and economic dispatch problem (EDP) of SG. A two-stage optimization approach is proposed in [7] to solve the problem of optimizing the VOP in the distribution network, the first stage uses an offline centralized algorithm to optimize the difference between the bus voltage at the pilot node (PN) and the reference value, and the second stage uses an online distributed algorithm to optimize the PN voltage in each weakly coupled voltage control zone. In [8], a novel voltage optimization procedure using a decentralized control strategy is proposed to optimize the VOP of a radially operating distribution system. In [9], the voltage quality of an N-stage neutral point clamped (NPC) inverter reconfigured after a fault is analyzed and an optimization method is proposed to mitigate the voltage quality degradation. [10] proposes a multi-level coordinated voltage control strategy based on a sensitivity approach for facilitating distributed residential demand response to optimize network voltage. With the aim of improving the safety and stability of high-voltage and medium-voltage distribution networks and achieving optimal operation of continuous and discrete voltage

regulation devices, [11] proposes a hierarchical distribution voltage optimization method. [12] designed a smart grid real-time distributed voltage control method to cope with the risk of voltage violation caused by the increased proportion of distributed energy access in SG. For EDP of MES, [13] proposes a distributed optimization algorithm with faster convergence speed and lower communication burden. [14] proposes a two-level optimization model for MES considering operational and carbon emission constraints, where the upper-level model studies the optimal resource allocation of MES and the lower-level model explores the stable operation of MES under low carbon emission. With respect to dynamic economic dispatch problem (DEDP) in SG scenarios, [15] proposes a new alternating direction method of multipliers algorithm based on distributed consistency theory. Based on the singular ingestion system and Hysteretic Q-learning, [16] proposes a novel distributed reinforcement learning solution to address EDP and DEDP in the SG context. In response to the prevalence of communication link delay in communication networks, [17] proposes a distributed economic scheduling protocol with constant delay to explore the impact of delay on scheduling performance. To effectively cope with the lack of prior knowledge of DEDP in SG, [18] proposes a new distributed reinforcement learning optimization algorithm. [19] investigates the problem of resource allocation for communication over strongly connected directed graphs and proposes a continuous-time projection algorithm that operates in a distributed manner. Based on EDP, [20] considers the demand response problem at the user side and discusses EMP with the goal of maximizing social welfare in the context of EI, as well as proposes a new distributed algorithm based on ADMM. On the basis of [20]'s work, [6] considers energy transactions of EI on directed graphs and proposes a new distributed algorithm based on the Newton method. In view of the existing ADMM convergence speed needs to be improved, [21] proposes a distributed optimization method with faster convergence speed and can effectively address the EMP of SG.

During the work mentioned above, various distributed algorithms have been well studied and developed for the optimization problem of MES and SG. Nevertheless, they do not consider that the cost functions and constraints formulated for energy supply devices in MES and SG may be described as non-smooth functions, and there are many time-varying factors in the actual system operation, neither do they discuss the stability of the formulated algorithms under time-varying problems. Consequently, in this paper, we focus on the EMP under time-varying conditions in the EI scenario and solve it in a fully distributed manner, which poses some challenges. From the optimization problem perspective, the strong coupling between multiple energy networks in EI and the need to fully consider the demand response problem at the user side make the formulation of the model difficult. From the algorithmic point of view, the proposed cost function and constraints are non-smooth functions and there are time-varying conditions in the constraints, which require good convergence and robustness of the proposed algorithm.

To tackle the above challenges, an optimization model for distributed energy management under multi-energy coupling is proposed, which contains nonsmooth cost functions and coupled inequality constraints, as well as time-varying loads. To address the EMP, we propose a distributed neurodynamic time-varying algorithm (DNTA) executed in a fully distributed manner. The following are the key contributions of this paper.

- In this paper, a model for EI in a time-varying load scenario is proposed for optimal energy allocation among EBs integrating renewable energy, flexible loads, and multi-energy coupling, while trading energy. The EMP is further formulated as a distributed time-varying optimization problem with non-smooth objective functions and constraints, allowing the intelligences in the EBs to perform their optimal operations locally.

- A neurodynamic algorithm implemented in a fully distributed manner that enjoys hardware implementation and parallel computation is proposed in this paper. The algorithm can effectively tackle EMPs with non-smooth objective functions and constraints under time-varying conditions. Moreover, experimental results indicate that the algorithm proposed in this paper exhibits better robustness and convergence speed compared to the work in [22, 23].

This paper is organized as follows. In Section 2, some basic concepts related to convex optimization are introduced. Section 3 outlines the mathematical model of EMP in the EI scenario. In Section 4, a distributed neurodynamic time-varying algorithm designed to tackle the EMP is presented. The results of the performance evaluation are provided in Section 5, and the conclusions of this paper are presented in Section 6.

2. Preliminaries

2.1. Graph theory

The messages exchanged between the agents in the communication network can be represented by $\mathcal{G} = (\mathcal{N}, \xi)$, where $\mathcal{N} = \{1, 2, \ldots, n\}$ is the set of nodes, and $\xi \subseteq \mathcal{N} \times \mathcal{N}$ is the set of edges. If $(j, i) \in \xi$ and agent j belongs to the set of neighbors of agent i $\mathcal{N} = \{j | (j, i) \in \xi\}$, then it means that agent i can obtain information from agent j. If and only if $(i, j) \in \xi$ and $(j, i) \in \xi$, $\mathcal{G}$ is called an undirected graph.

Define the adjacency matrix of a graph $\mathcal{G}$ as $A = [a_{ij}]$ with $a_{ij} = 1$ if $j \in \mathcal{N}$ and $a_{ij} = 0$ otherwise. The Laplacian matrix of a graph $\mathcal{G}$ is $\mathcal{L} = D - A$, where D is the degree matrix of A and is a diagonal matrix composed of $D_{ii} = \sum_{j=1}^{n} a_{ij}$.

2.2. Projection operator

Definition of the projection operator as

$$P_{\Omega}(\varsigma) = \arg \min_{\sigma \in \Omega} \|\varsigma - \sigma\|$$

One can obtain the following properties about $P_{\Omega}(\varsigma)$.

Lemma 1 ([24]). *Suppose Ω is the closed convex set, in which case the following inequality with respect to P holds.*

$$(P_{\Omega}(\varsigma) - \varsigma)^T (P_{\Omega}(\varsigma) - \sigma) \leq 0, \varsigma \in \mathfrak{R}^m, \sigma \in \Omega, \tag{1}$$

$$(P_{\Omega}(\varsigma) - P_{\Omega}(\sigma))^T (\varsigma - \sigma) \geq \|\varsigma - \sigma\|_2, \varsigma \in \mathfrak{R}^m, \sigma \in \Omega. \tag{2}$$

2.3. Nonsmooth analysis

The differential inclusion is defined as follows:

$$\dot{x}(t) \in \Gamma(t, x(t)), \ x(0) = x_0, \ t \geq 0, \tag{3}$$

where Γ is a set-valued mapping to a compact, non-empty, convex subset. When the solution of (3) defined on $[0, \tau] \subset [0, \infty)$ is an absolutely continuous function $x : [0, \tau] \to \mathfrak{R}^m$, the system (3) holds for almost all $t \in [0, \tau]$ with $\tau > 0$. Define $x^* \in \mathfrak{R}^m$ to be the equilibrium point of (3) and such that $0_m \in \Gamma(x^*)$. If and only if the constant function $x(\cdot) = x^*$ is a solution of (3), x^* is the equilibrium point of (3). Denote $x : [0, +\infty) \to \mathfrak{R}^m$ as a solution of (3), then if χ is a cluster point of $x(t)$ and also a Lyapunov stable equilibrium of (3), it follows that $\lim_{t \to \infty} x(t) = \chi$.

Lemma 2 ([25]). *Let Γ be a set-valued mapping from $\mathfrak{R}^m$ to $\mathfrak{R}^m$. Ω is a closed convex subset and N_{Ω} is the normal cone of Ω at x. It is a solution of (5) if and only if $x(\cdot)$ is a solution of (4).*

$$\dot{x} \in \Gamma(x) - N_{\Omega}(x), \ x(0) = x_0 \in \Omega, \tag{4}$$

$$\dot{x} \in P_{\Omega}(x - \Gamma(x)) - x, \ x(0) = x_0 \in \Omega. \tag{5}$$

Assume that V is locally Lipschitz continuous and let $\partial V(z)$ be denoted as the Clark's generalized gradient of $V(z)$ at z. V with respect to the set-valued Lie derivative $L_\Gamma V$ of the function Γ is defined as $L_\Gamma V := \{\ell \in \Re : \text{exists } a \in \Gamma(z) \text{ such that } v^T a = \ell \text{ for all } v \in \partial V\}$. The maximum element of $L_\Gamma V$ is denoted by $\max L_\Gamma V$ when $L_\Gamma V$ is non-empty. Assuming that $\varphi(\cdot)$ is a solution of (3) and that V is locally Lipschitz and regular, then $\dot{V}(\varphi(t))$ exists at any point and $\dot{V}(\varphi(t)) \in L_\Gamma V(\varphi(t))$ holds.

The following lemma gives the invariance principle for nonsmooth regular functions.

Lemma 3 ([26]). *In the case of* (3)*, it is assumed that Γ is upper semicontinuous and locally bounded, and $\Gamma(x)$ takes compact, nonempty and convex values. Suppose V is a function of local Lipschitz and regularity, H is strongly invariant and compact to* (3)*, and A is denoted as a solution of* (1)*. $R = \{x \in \Re^m : 0 \in L_\Gamma V(x)\}$. Define M to be denoted as the largest weakly invariant subset of $\bar{R} \cap H$, where $\bar{R}$ is the closure of R. If $\max L_\Gamma V \leq 0$ for all $x \in H$, and then $\text{dist}(\varphi(t), M) \to 0$ as $t \to +\infty$.*

2.4. Convex analysis

If the function $f : \Re^m \to \Re$ satisfies $f(\theta x + (1-\theta)y) \leq \theta f(x) + (1-\theta)f(y)$ for all $x, y \in \Re^m$ and $\theta \in [0,1]$, then $f : \Re^m \to \Re$ is a convex function. If the function $f : \Re^m \to \Re$ satisfies $f(\theta x + (1-\theta)y) \leq \theta f(x) + (1-\theta)f(y)$ for all $x, y \in \Re^m$, $x \neq y$ and $\theta \in (0,1)$, then $f : \Re^m \to \Re$ is a strongly convex function. $\partial f(x)$ denotes the subdifferential of $f(x)$ at $x \in \Re^m$ that is defined as $\partial f(x) := \{g \in \Re^m : g^T(x-y) \leq f(x) - f(y) \text{ for all } y \in \Re^m\}$ and the element of $\partial f(x)$ is called the subgradient of $f(x)$ at point x. The $(\partial f(x) - \partial f(y))^T(x-y) > 0$ can be easily obtained by the properties of strictly convex functions.

3. Problem formulation

To facilitate the delineation of the different regions, EI is considered to be composed of multiple energy bodies (EBs), whose structure is presented in Fig. 1. Seen from different application scenarios, in case EI is considered as a city, EB may be one of the towns; in case EI is considered as a town, EB may be one of its communities. Each EB operates in island mode or interconnected mode, where EBs are connected through energy and communication networks, and enable energy transactions and information interaction with their neighbor EBs. The interior of EB is composed of multiple energy supply units and energy loads (ELs). The energy supply units are mainly composed of fuel generators (FG), renewable energy generators (REG), power storage equipment (PSE), combine heat and power (CHP), fuel boilers (FB), renewable heating equipment (REHU), heat storage equipment (HSE) and natural gas suppliers (NGS). ELs are composed of electricity load, heat load and gas load, and each load is composed of equivalent flexible load and fixed load. Energy networks and communication networks in EI are considered as actual networks. And there are interactions of energy and information among EBs in EI, so several different EIs interconnected actually form a larger EI.

3.1. EB model

3.1.1. Cost function

To facilitate the description of the model of EI, we use an agent to represent the energy supply unit or EL in the EB.

(1). Both FG and FB burn fuel to obtain electric or heat, and their cost functions are mainly used to describe the cost of fuel and the cost of treating the emitted polluted gas. FG cost functions can be modeled as

$$C_{ij}^{pf}\left(p_{ij}^f\right) = a_{ij}^f\left(p_{ij}^f\right)^2 + b_{ij}^f p_{ij}^f + r_{ij}^f \exp\left(u_{ij}^f p_{ij}^f\right) \tag{6}$$

where p_{ij}^f represents the active power output of FG labeled j in the ith EB; a_{ij}^f and b_{ij}^f are positive cost coefficients; exp function represents the
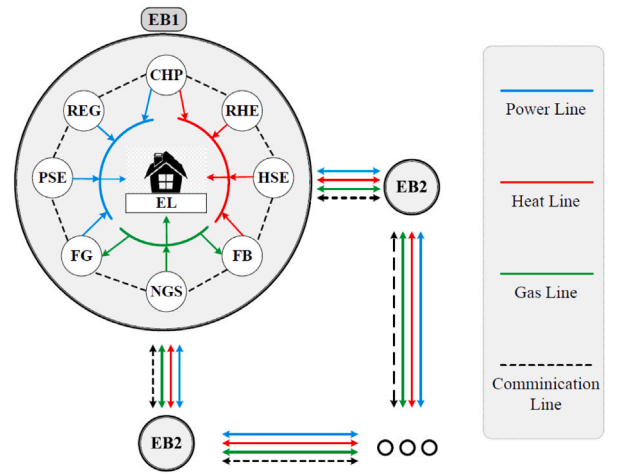

Fig. 1. System architecture of EI.

penalty for treating polluted gas; r_{ij}^f and u_{ij}^f are penalty parameters. Just like FG, the cost function of FB can be modeled as

$$C_{ij}^{hf}\left(h_{ij}^f\right) = \alpha_{ij}^f\left(h_{ij}^f\right)^2 + \beta_{ij}^f h_{ij}^f + \gamma_{ij}^f \exp\left(\mu_{ij}^f h_{ij}^f\right) \tag{7}$$

where h_{ij}^f is the heating power of FB labeled j in the ith EB; α_{ij}^f and β_{ij}^f are positive cost coefficients; exp function represents the penalty for treating polluted gas; γ_{ij}^f and μ_{ij}^f are positive penalty parameters.

(2). The cost of REG and RHE with renewable energy as input mainly comes from the maintenance of labor and equipment. The REG cost function is

$$C_{ij}^{pr}\left(p_{ij}^r\right) = b_{ij}^r p_{ij}^r + r_{ij}^r \exp\left(u_{ij}^r \frac{p_{ij}^{r,\max} - p_{ij}^r}{p_{ij}^{r,\max} - p_{ij}^{r,\min}}\right) \tag{8}$$

where p_{ij}^r represents the active power output of REG labeled j in the ith EB; b_{ij}^r is a positive cost coefficient; exp function is used to balance the feasibility and optimality of REG power supply; r_{ij}^r and u_{ij}^r are positive coefficients; $p_{ij}^{r,\max}$ and $p_{ij}^{r,\min}$ are the feasible maximum and minimum values of p_{ij}^r, respectively. In the same way, the cost function of RHE can be defined as

$$C_{ij}^{hr}\left(h_{ij}^r\right) = \beta_{ij}^r h_{ij}^r + \gamma_{ij}^r \exp\left(\mu_{ij}^r \frac{h_{ij}^{r,\max} - h_{ij}^r}{h_{ij}^{r,\max} - h_{ij}^{r,\min}}\right) \tag{9}$$

where h_{ij}^r is the heating power output of RHE labeled j in the ith EB; β_{ij}^r is positive cost coefficient; The feasibility and optimality of exp function for balancing RHE heating; γ_{ij}^r and μ_{ij}^r are positive coefficients. The feasible Maximum and minimum values of h_{ij}^r are expressed by $h_{ij}^{r,\max}$ and $h_{ij}^{r,\min}$, respectively.

(3). Similar to FG and FB, the cost of CHP mainly comes from fuel, and its cost function is

$$C_{ij}^c\left(p_{ij}^c, h_{ij}^c\right) = a_{ij}^c\left(p_{ij}^c\right)^2 + b_{ij}^c p_{ij}^c + \kappa_{ij}^c p_{ij}^c h_{ij}^c$$
$$+ \beta_{ij}^c h_{ij}^c + \alpha_{ij}^c\left(h_{ij}^c\right)^2 + l_{ij}^c \tag{10}$$

where p_{ij}^c and h_{ij}^c are the active power output and heating power of CHP labeled j in the ith EB, respectively; a_{ij}^c, b_{ij}^c, κ_{ij}^c, β_{ij}^c, α_{ij}^c and l_{ij}^c are positive cost factors.

(4). Major users of energy storage devices balance the randomness and volatility of renewable energy and load. Instead, in the process of energy storage and release, there will inevitably be some loss. Construct the following cost function to describe the loss of PSE

$$C_{ij}^{ps}\left(p_{ij}^s\right) = b_{ij}^s\left|p_{ij}^s\right| + a_{ij}^s\left(p_{ij}^s\right)^2 + \varsigma^p p_{ij}^s \tag{11}$$

where p_{ij}^s is the active power of the PSE labeled j in the ith EB; b_{ij}^s and a_{ij}^s are positive cost coefficient and loss coefficient respectively; ς^p is electricity price. Construct the following cost function to describe the loss of HSE.

$$C_{ij}^{hs}\left(h_{ij}^s\right) = \beta_{ij}^s \left|h_{ij}^s\right| + \varsigma^h h_{ij}^s + \gamma_{ij}^s \exp\left(\mu_{ij}^s \frac{h_{ij}^{s,\max} - h_{ij}^s}{h_{ij}^{s,\max} - h_{ij}^{s,\min}}\right) \tag{12}$$

where h_{ij}^s represents the thermal power of HSE labeled j in the ith EB; β_{ij}^s is a positive loss coefficient; ς^h is the heat price; Feasibility and optimality of exp function used to balance heat storage; γ_{ij}^s and μ_{ij}^s are positive coefficients.

(5). The cost function of NGS is [20]

$$C_{ij}^g\left(g_{ij}\right) = a_{ij}^g g_{ij}^3 + b_{ij}^g g_{ij}^2 + c_{ij}^g g_{ij} + v_{ij}^g \tag{13}$$

where g_{ij} is the output gas power of NGS labeled j in the ith EB; a_{ij}^g, b_{ij}^g, c_{ij}^g and v_{ij}^g are non-negative cost factors.

3.1.2. Utility function

(1). EL is regarded as an equivalent flexible load that can be scheduled and an uncontrollable fixed load [27]. Flexible load is considered as the load of public utilities, which can be transferred to a certain extent. Fixed load is considered as the load of the vast number of users, which is difficult to control. We use the following benefit function to describe the scheduling of flexible load

$$U_i^L\left(t, e_i^p, e_i^h, e_i^g\right) = U_i^{lp}\left(t, e_i^p\right) + U_i^{lh}\left(t, e_i^h\right) + U_i^{lg}\left(t, e_i^g\right) \tag{14}$$

$$\begin{cases} U_i^{lp}\left(t, e_i^p\right) = a_i^p\left(e_i^p\right)^2 - b_i^p\left(e_i^p + \ell_i^p(t)\right) \\ U_i^{lh}\left(t, e_i^h\right) = a_i^h\left(e_i^h\right)^2 - b_i^h\left(e_i^h + \ell_i^h(t)\right) \\ U_i^{lg}\left(t, e_i^g\right) = a_i^g\left(e_i^g\right)^2 - b_i^g\left(e_i^g + \ell_i^g(t)\right) \end{cases}$$

where e_i^p, e_i^h and e_i^g are equivalent flexible loads of electricity, heat and gas, respectively; $\ell_i^p(t)$, $\ell_i^h(t)$ and $\ell_i^g(t)$ are equivalent fixed loads of time-varying electricity, heat and gas respectively; a_i^p, a_i^h, a_i^g, b_i^p, b_i^h and b_i^g are negative benefit coefficients.

Remark 1. During a dispatch period, the value of fixed load is generally predicted based on historical data, but in practical application scenarios, the value of fixed load fluctuates with time. In addition, uncontrollable equipment failure, line damage and other factors will cause the load to change drastically in a short time. Therefore, it is more practical to describe the fixed load as a time-varying value.

(2). The EBs have mutual energy transactions, and a single EB will have some local energy supply and demand mismatch (surplus or shortage). The energy mismatch in a single EB is defined as

$$\begin{cases} \mathbf{p}_i^\mathbf{m}(t) = p_{ij}^f + p_{ij}^r + p_{ij}^c + p_{ij}^s - e_i^p - \ell_i^p(t) \\ \mathbf{h}_i^\mathbf{m}(t) = h_{ij}^f + h_{ij}^r + h_{ij}^c + p_{ij}^s - e_i^h - \ell_i^h(t) \\ \mathbf{g}_i^\mathbf{m}(t) = g_{ij} - e_i^g - \ell_i^g(t) \end{cases}$$

During the transaction, EB will generate certain profit or deficit. The following benefit function is used to describe the energy transaction between EBs.

$$U_i^R = \varsigma^p \mathbf{p}_i^\mathbf{m}(t) + \varsigma^h \mathbf{h}_i^\mathbf{m}(t) + \varsigma^g \mathbf{g}_i^\mathbf{m}(t) \tag{15}$$

3.1.3. System operating constraints

(1). Capacity constraints: The active power of FG, REG and PSE shall meet the following capacity constraints

$$0 < p_{ij}^{f,\min} \leq p_{ij}^f \leq p_{ij}^{f,\max} \tag{16}$$

$$0 < p_{ij}^{r,\min} \leq p_{ij}^r \leq p_{ij}^{r,\max} \tag{17}$$

$$\left|p_{ij}^s\right| \leq p_{ij}^{s,\max} \tag{18}$$

where $p_{ij}^{f,\max}$ and $p_{ij}^{f,\min}$ are the feasible upper and lower limits of the active power of p_{ij}^f, respectively; $p_{ij}^{s,\max}$ is the maximum charge and discharge power.

The power supply and heating power of CHP shall meet the following linear inequality constraints

$$u_{ij,k}^1 p_{ij}^c + u_{ij,k}^2 h_{ij}^c + u_{ij,k}^3 \leq 0, k = 1, 2, 3 \tag{19}$$

where $u_{ij,k}^1$, $u_{ij,k}^2$ and $u_{ij,k}^3$ are positive power limiting coefficients.

The heating power of FB, REHU and HSE shall meet the following capacity limits

$$0 < h_{ij}^{f,\min} \leq h_{ij}^f \leq h_{ij}^{f,\max} \tag{20}$$

$$0 < h_{ij}^{r,\min} \leq h_{ij}^r \leq h_{ij}^{r,\max} \tag{21}$$

$$\left|h_{ij}^s\right| \leq h_{ij}^{s,\max} \tag{22}$$

where $h_{ij}^{f,\max}$ and $h_{ij}^{f,\min}$ are the upper and lower bounds of the feasible power of h_{ij}^f, respectively; $h_{ij}^{s,\max}$ is the maximum heat storage and heat dissipation power.

The output of NGS should meet

$$0 \leq g_{ij}^{\min} \leq g_{ij} \leq g_{ij}^{\max} \tag{23}$$

where $g_{ij}^{\max}$ and $g_{ij}^{\min}$ represent the maximum and minimum natural gas output power respectively.

(2). Ramp rate constrains: In PSE and HSE, the power ramp rate constraint in the process of energy storage and release can be described as

$$-p_{ij,\tau}^{s,ra} \leq -p_{ij,\tau}^s - p_{ij,\tau-1}^s \leq p_{ij,\tau}^{s,ra} \tag{24}$$

$$-h_{ij,\tau}^{s,ra} \leq -h_{ij,\tau}^s - h_{ij,\tau-1}^s \leq h_{ij,\tau}^{s,ra} \tag{25}$$

where $p_{ij,\tau}^{s,ra}$ and $h_{ij,\tau}^{s,ra}$ are ramp rate constraints of PSE and HSE, respectively.

(3). Flexible load scheduling constraints: The feasible interval of schedulable flexible constraints is

$$0 \leq e_i^p \leq e_i^{p,\max} - \ell_i^p(t) \tag{26}$$

$$0 \leq e_i^h \leq e_i^{h,\max} - \ell_i^h(t) \tag{27}$$

$$0 \leq e_i^g \leq e_i^{g,\max} - \ell_i^g(t) \tag{28}$$

where $e_i^{p,\max}$, $e_i^{h,\max}$ and $e_i^{g,\max}$ are the maximum schedulable flexible electrical load, flexible thermal load and flexible gas load, respectively.

(4). Energy transmission line constraint: Power supply network, heating network and gas supply network are prone to congestion on some lines when transmitting energy. The following nonlinear constraints are used to describe the line congestion limit.

$$\sum_{i=1}^n \sum_{j=1}^m \rho_{ij}^{pf}\left|p_{ij}^f\right| + \rho_{ij}^{pr}\left|p_{ij}^r\right| + \rho_{ij}^{pc}\left|p_{ij}^c\right| + \rho_{ij}^{ps}\left|p_{ij}^s\right| \leq P_l \tag{29}$$

$$\sum_{i=1}^n \sum_{j=1}^m \rho_{ij}^{hf}\left|h_{ij}^f\right| + \rho_{ij}^{hr}\left|h_{ij}^r\right| + \rho_{ij}^{hc}\left|h_{ij}^c\right| + \rho_{ij}^{hs}\left|h_{ij}^s\right| \leq H_l \tag{30}$$

$$\sum_{i=1}^n \sum_{j=1}^m \rho_{ij}^{gs}\left|g_{ij}^s\right| \leq G_l \tag{31}$$

where ρ_{ij}^{pf}, ρ_{ij}^{pr}, ρ_{ij}^{pc} and ρ_{ij}^{ps} are non-negative electric power coefficients, and P_l is the congestion limit of transmission lines; ρ_{ij}^{hf}, ρ_{ij}^{hr}, ρ_{ij}^{hc} and ρ_{ij}^{hs} are non-negative heating power coefficients, and H_l is the line congestion limit of heating network; g_{ij} is a non-negative gas supply power coefficient, and G_l is the congestion limit of gas supply pipeline.

3.2. Problem statement

With regard to EI, the EMP is described as the search for the overall lowest operating cost of EI while satisfying the supply–demand balance of each energy network, the power constraints of each energy supply

unit/EL, and the transmission line congestion constraints. It is defined as follows

$$\min \sum_{i=1}^{n} \sum_{j=1}^{m} \left(C_{ij}^{pf} + C_{ij}^{hf} + C_{ij}^{pr} + C_{ij}^{hr} + C_{ij}^{ps} \right.$$

$$\left. + C_{ij}^{hs} + C_{ij}^{g} \right) - U_i^L - U_i^R \right) \tag{32a}$$

$$s.t. \sum_{i=1}^{n} \mathbf{p}_i^{\mathbf{m}}(t) = \mathbb{0}, \sum_{i=1}^{n} \mathbf{h}_i^{\mathbf{m}}(t) = \mathbb{0}, \sum_{i=1}^{n} \mathbf{g}_i^{\mathbf{m}}(t) = \mathbb{0} \tag{32b}$$

$$and \; (16)–(31) \tag{32c}$$

where n indicates that the EI consists of n EBs, the m represents the maximum number of agents in the EB, and $\mathbb{0}$ denotes the zero vector of the corresponding dimension.

For simplifying the description, we use more concise symbols to describe the EMP of EI. The 3-dimensional vector $x_{ij} \in \mathbb{R}^3$ represents the power output of each energy supply unit or the flexible load of EL, and is distinguished by ω_{ij}. When x_{ij} represents the flexible load, ω_{ij} is $-I_3$, otherwise it is I_3. Let $\Phi(x,t)$ represents the cost function or utility function, and the set Ω_{ij} represents the constraint (16)–(28). Divide the multi-energy fixed load of the ith EB into m parts equally, and define $\ell_{ij}(t) \in \mathbb{R}^3$ as a three-dimensional vector composed of the jth multi-energy fixed load of the ith EB. And let $\varphi_{ij}(x_{ij})$ represent the congestion constraint of the jth nonlinear transmission line of the ith EB. Eventually, EMP (32) is simplified to the following time-varying optimization problem.

$$\min \Phi(x,t) = \sum_{i=1}^{n} \sum_{j=1}^{m} \Phi_{ij}(x,t) \tag{33a}$$

$$s.t. \sum_{i=1}^{n} \sum_{j=1}^{m} \omega_{ij} x_{ij} = \sum_{i=1}^{n} \sum_{j=1}^{m} \ell_{ij}(t) \tag{33b}$$

$$\sum_{i=1}^{n} \sum_{j=1}^{m} \varphi_{ij}(x_{ij}) \leq \mathbb{0} \tag{33c}$$

$$x_{ij} \in \Omega_{ij} \tag{33d}$$

4. Distributed algorithm

Noted that EMP (32) is a time-varying optimization problem with time-varying conditions and nonsmooth objective functions and constraints, which places higher demands on the performance of the algorithm. Accordingly, we propose the following distributed neural dynamics time-varying algorithm (DNTA) to track the optimal solution of the EMP in a fully distributed manner.

$$\varepsilon \dot{x}_{ij} \in \mathcal{P}_{\Omega_{ij}} \left(x_{ij} - \partial \Phi_{ij}(x_{ij}) + \omega_{ij}^T \lambda_{ij} - \partial \varphi_{ij}^T(x_{ij}) \mathcal{P}_+^{\eta_{ij}} \right)$$

$$- x_{ij} \tag{34a}$$

$$\varepsilon \dot{\lambda}_{ij} = \ell_{ij}(t) - \omega_{ij}(x_{ij} + \dot{x}_{ij}) - \sigma \sum_{i\bar{j} \in \mathcal{N}} a_{ij,i\bar{j}} \left(\lambda_{ij} - \lambda_{i\bar{j}} \right)$$

$$- \sigma \sum_{i\bar{j} \in \mathcal{N}} a_{ij,i\bar{j}} \left(y_{ij} - y_{i\bar{j}} \right) \tag{34b}$$

$$\varepsilon \dot{y}_{ij} = \sigma \sum_{i\bar{j} \in \mathcal{N}} a_{ij,i\bar{j}} \left(\lambda_{ij} - \lambda_{i\bar{j}} \right) \tag{34c}$$

$$\varepsilon \dot{\eta}_{ij} \in \mathcal{P}_+^{\eta_{ij}} - \eta_{ij} \tag{34d}$$

$$\varepsilon \dot{z}_{ij} = \sigma \sum_{i\bar{j} \in \mathcal{N}} a_{ij,i\bar{j}} \left(\mathcal{P}_+^{\eta_{ij}} - \mathcal{P}_+^{\eta_{i\bar{j}}} \right) \tag{34e}$$

$$\mathcal{P}_+^{\eta_{ij}} = \left[\varphi_{ij}(x_{ij}) - \sigma \sum_{i\bar{j} \in \mathcal{N}} a_{ij,i\bar{j}} \left(\mathcal{P}_+^{\eta_{ij}} - \mathcal{P}_+^{\eta_{i\bar{j}}} \right) \right.$$

$$\left. - \sigma \sum_{i\bar{j} \in \mathcal{N}} a_{ij,i\bar{j}} \left(z_{ij} - z_{i\bar{j}} \right) + \partial \varphi_{ij}^T(x_{ij}) \dot{x}_{ij} \right]_+^{\eta_{ij}} \tag{34f}$$
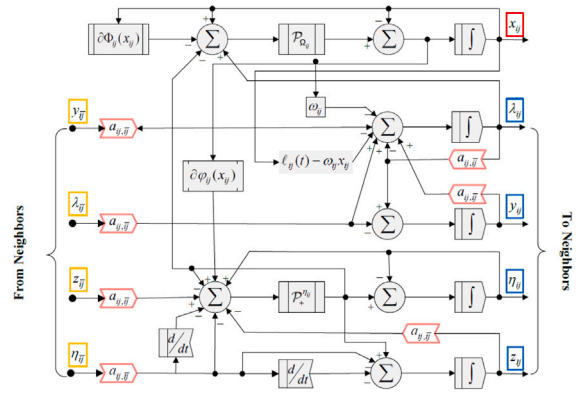

Fig. 2. Internal logic design of DNTA (34).

where λ, y, η and z are Lagrange multipliers that assist the decision variable x to converge to the optimal trajectory; ε and σ are positive bounded gains, which can effectively improve the convergence speed and stability of the algorithm; $\mathcal{P}_{\Omega_{ij}}(s)$ is the projection of s to the set Ω_{ij}, ensuring that x converges to the set Ω_{ij}; $\mathcal{P}_+^{\eta_{ij}}(s)$ is the positive projection of s onto a non-negative real number field, i.e. $\mathcal{P}_+^{\eta_{ij}}(s) = s$ for $\eta_{ij} > 0$ or $s < 0$, otherwise $\mathcal{P}_+^{\eta_{ij}}(s) = 0$; $\partial \Phi_{ij}(x_{ij})$ and $\partial \varphi_{ij}(x_{ij})$ are the subdifferentials for $\Phi_{ij}(x_{ij})$ and $\varphi_{ij}(x_{ij})$, respectively.

Fig. 2 depicts the internal logic design of DNTA, which can also be seen as the computational logic of an agent labeled as ij. As can be seen from the figure, the agent labeled ij exchanges information about the multipliers (λ, y, η, z) with the neighboring agents. The decision variable x, on the other hand, is only computed locally and is not exchanged with other agents. This effectively protects the privacy of each agent and reduces the communication requirements. To conveniently describe the implementation flow of the algorithm, the DNTA is discretized using the Euler method, i.e., a suitable step size v is chosen such that $s_{k+1} = s_k - v(\partial F(s_k))$ is equivalent to $\dot{s} = \partial F(s)$. The flow chart of the implementation of algorithm (34) is illustrated in Fig. 3. In preparation, the relevant parameters of the objective function and constraints as well as the communication connectivity among the agents are determined. Firstly, take arbitrary bounded initial values for the all variables $(x_{ij}, \lambda_{ij}, y_{ij}, \eta_{ij}, z_{ij})$. Let the number of updates k be 0 and the Lagrange multipliers $(\lambda_{ij}, y_{ij}, \eta_{ij}, z_{ij})$ exchange information with their neighbors. Then the variables take parallel computation and are updated corresponding to the Eulerian discrete versions of (34a), (34b), (34c), (34d) and (34d), respectively. The algorithm stops updating when all variables converge, otherwise the number of updates is increased by one and the update operation is repeated.

Remark 2. The proposed algorithm DNTA decouples the coupling constraints in a fully distributed manner with favorable robustness and stability. With the concept of subgradient and differential inclusion, the DNTA is able to tackle non-smooth objective functions and constraints. With respect to $\omega_{ij} \dot{x}_{ij}$ and $\partial \varphi_{ij}^T(x_{ij})\dot{x}_{ij}$ in Eqs. (34b) and (34d). From the control point of view they are based on differential feedback design and act as damping terms; from the optimization point of view, they help λ_{ij} and η_{ij} point to the future direction of motion and have a predictive role. Therefore, DNTA has the ability to track the time-varying optimal trajectory of EMP (see Fig. 3).

Define $x = [x_{11}^T, \ldots, x_{nm}^T]^T$ and define the λ, y, η, z, ω and $\ell(t)$ in the same way. Let $\mathcal{L}$ be the Laplacian matrix of the communication connectivity graph $\mathcal{G}$ of agents. The compact form of DNTA is expressed as follows

$$\varepsilon \dot{x} \in \mathcal{P}_{\hat{\Omega}} \left(x - \partial \Phi(x) + \omega^T \lambda - \partial \varphi^T(x) \mathcal{P}_+^{\eta} \right) - x \tag{35a}$$

$$\varepsilon \dot{\lambda} = \ell(t) - \omega(x + \dot{x}) - \sigma \mathcal{L} \lambda - \sigma \mathcal{L} y \tag{35b}$$
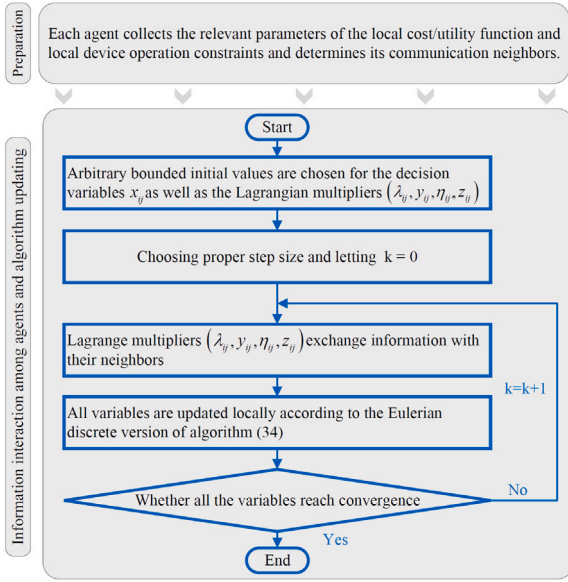
Fig. 3. Algorithm implementation flow chart for Eulerian discrete version of DNTA (34).

$$\varepsilon \dot{y} = \sigma \mathcal{L} \lambda \tag{35c}$$

$$\varepsilon \dot{\eta} \in \mathcal{P}_+^{\eta} - \eta \tag{35d}$$

$$\varepsilon \dot{z} = \sigma \mathcal{L} \mathcal{P}_+^{\eta} \tag{35e}$$

$$\mathcal{P}_+^{\eta} = \left[\varphi(x) + \partial \varphi^T(x)\dot{x} - \sigma \mathcal{L} \mathcal{P}_+^{\eta} - \sigma \mathcal{L} z \right]_+^{\eta} \tag{35f}$$

Theorem 1. *Suppose the problem* (33) *always has an optimal trajectory within the constraints, and the graph $\mathcal{G}$ is undirected connected at any moment.*

(i). *There exists* $(\lambda^*, y^*, \eta^*, z^*)$ *such that* $(x^*, \lambda^*, y^*, \eta^*, z^*)$ *is the equilibrium trajectory of the DNTA* (35) *when and only when the optimal trajectory of the problem* (33) *is* x^*.

(ii). *The DNTA* (35) *is globally stable in the sense of Lyapunov, and x will converge to the optimal trajectory of the problem* (33).

See appendix for the proof of Theorem 1.

5. Simulation performance results

The performance of DNTA in a simulated EI test system is tested in a simulation experiment. Fig. 4 depicts the layout of the test system for EI with four EBs. The test parameters for each energy supply device and EL are given by [20].

5.1. Stability performance analysis

In the case 1 study, the convergence of DNTA in 20 s is first tested to demonstrate the stability of the algorithm. Fig. 5 depicts the generation/consumption of the 4 EBs under load determination, and it is easy to see from subplots (a), (b), (c), and (d) that the estimated generation/consumption trajectories of all agents in the 4 EBs tend to be stable within $2s$. In addition, the four subplots of Fig. 6 show the heat generation/consumption in each of the 4 EBs. Fig. 7 demonstrates the gas generation/consumption of all EBs, where EL_1 indicates the gas energy consumption of EL in EB1; NGS_4 indicates the gas generation of NGS in EB4; and the same for the others.

We visualize the optimal operation performed by each agent using the energy mismatches $\sum_{i=1}^{n} \mathbf{p}_i^{\mathbf{m}}(t)$, $\sum_{i=1}^{n} \mathbf{h}_i^{\mathbf{m}}(t)$ and $\sum_{i=1}^{n} \mathbf{g}_i^{\mathbf{m}}(t)$ for electricity, heat and gas, and the experimental results are shown in Fig. 8.
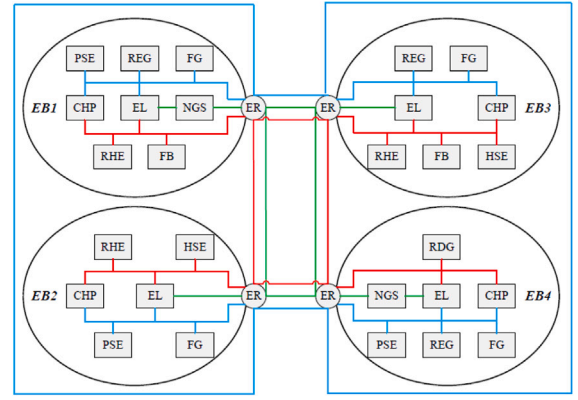

Fig. 4. EI system with four EBs.

(a) Situation in EB1.

(b) Situation in EB2.

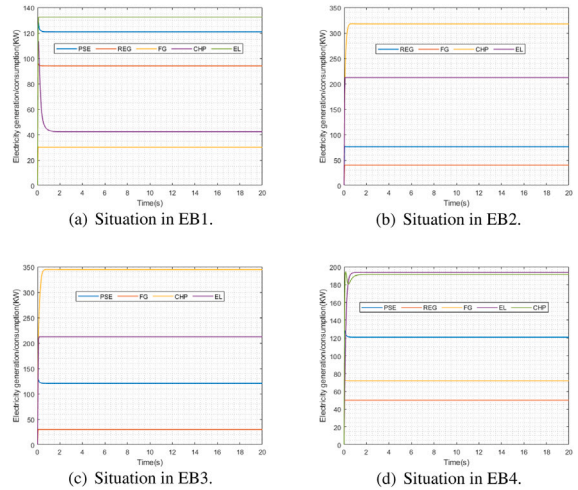(c) Situation in EB3.

(d) Situation in EB4.

Fig. 5. Simulation results of electricity generation/consumption.

It is clear from the figure that the mismatch of the three energy sources tends to zero within 1s, which reflects that the operation performed by each agent makes the demand of the load to be satisfied.

In addition, in the EI scenario, energy trading is possible among EBs, and EBs with local energy surpluses are allowed to sell energy to EBs with local energy deficits. Figs. 9–11 demonstrate the trading among EBs, with positive values indicating the profit gained during the trading process and negative values the expenditure for purchasing energy. The experimental results reveal that the DNTA proposed in this paper has favorable stability.

5.2. Robust performance analysis

During the operation of the EI system, some undesirable factors may cause impacts on the stable operation of the system, such as blocked communication, line failure and equipment damage. For this reason, in the case 2 study, we tested the robustness of DNTA with the same parameters as case 1 except for the communication connection relationship and load.

Firstly, the robustness of DNTA in case of communication blockage is tested. To perform the test, the communication network among the agents is assumed to change abruptly under the influence of undesirable factors, and the mutating communication networks is presented in Fig. 12. In the simulation experiments, to visualize the results, energy mismatch is used to demonstrate the performance of DNTA in the changing communication network. Communication link 1 is used between the EBs at moment $t1$, communication link 2 is used
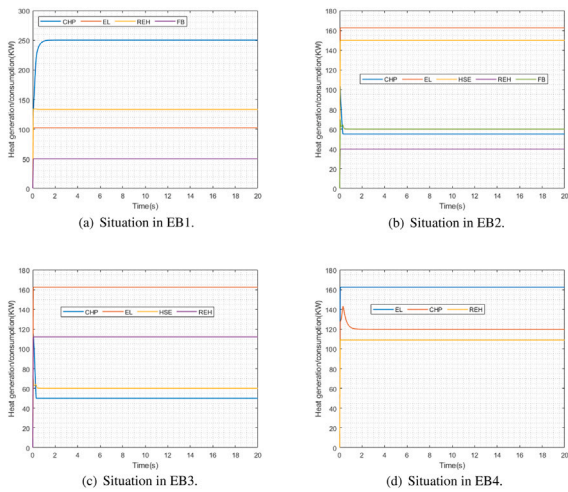
(a) Situation in EB1.

(b) Situation in EB2.

(c) Situation in EB3.

(d) Situation in EB4.

Fig. 6. Simulation results of heat generation/consumption.
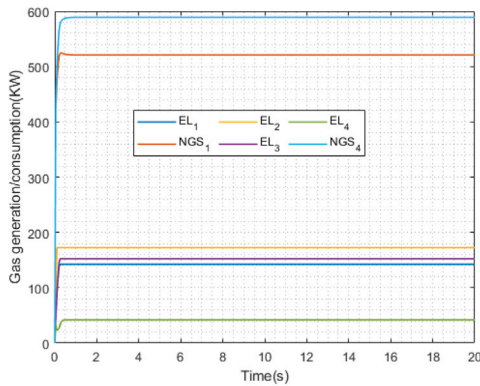
Fig. 7. Simulation results of gas generation/consumption.

Fig. 8. Energy mismatch.

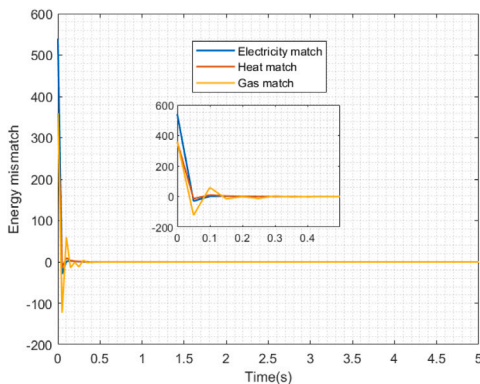**Fig. 9.** Electricity trading.

Fig. 10. Heat trading.

Fig. 11. Gas trading.

between moment $t1$ and moment $t2$, and communication link 3 is used after moment $t2$. The experimental results are presented in Fig. 13, which shows that the energy mismatch fluctuates briefly at moment $t1$ and after moment $t2$ affected by the change of the communication network, but soon converges to zero again. It is worth noting that energy mismatch reflects whether the energy supply unit effectively meets the demand of the load. Overall, although energy storage devices are capable of storing a certain amount of excess energy, a large-scale energy mismatch over a long period of time will inevitably result in a large amount of wasted resources and may also cause energy disconnection, i.e., power and gas outages, which seriously affects
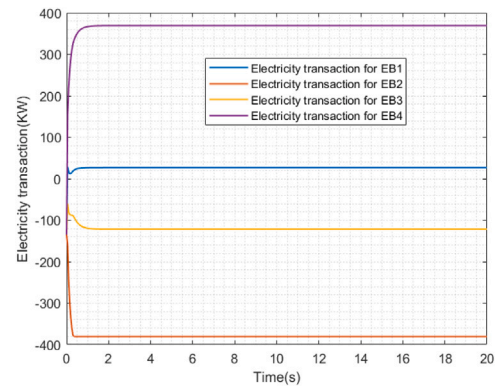
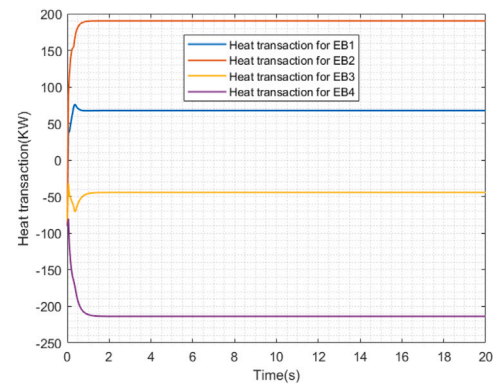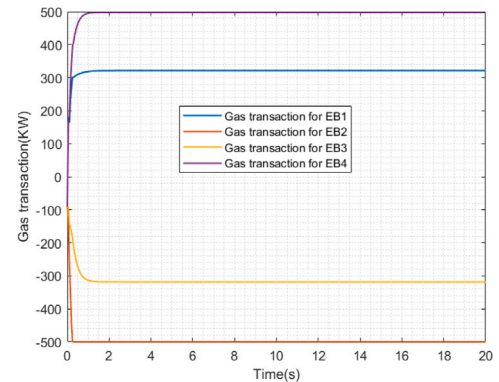the economy and safety of the system. And the algorithm may lead to failure and non-convergence if it cannot adapt to the mutating communication network in a short time. The proposed DNTA maintains favorable effectiveness even in the mutating communication network, and minimizes the adverse effects on the system operation.

After that, the performance of DNTA in terms of plug-and-play is tested. Assume that PSE and FB in EB1 and FG in EB3 are suddenly disconnected from the system due to line failure and equipment damage. The experimental results are depicted in Figs. 14–15, from which it can be seen that after $10s$, the electrical power of PSE and the heat power of FB in EB1 and the heat power of FG in EB3 drop to 0. At the same time, the production/consumption of other energy supply devices and EL are adaptively changed to compensate for the power gap caused by the sudden disconnection of the devices, and finally converge to a new optimal operation. As can also be seen from the energy
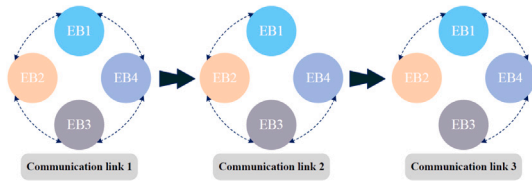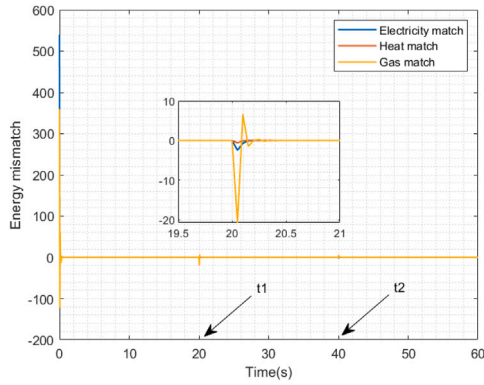
Fig. 12. Mutating communication networks.

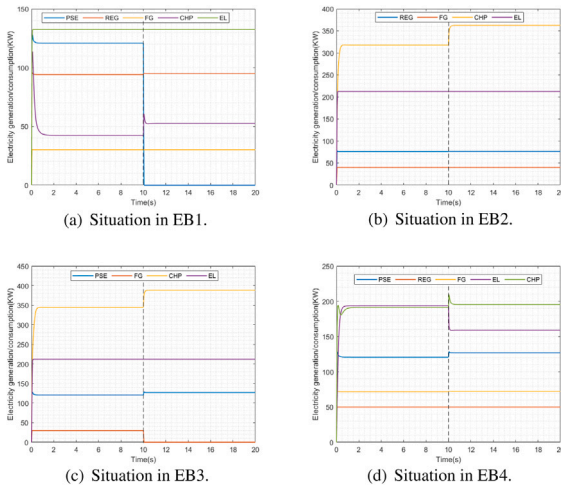Fig. 13. Energy mismatch under mutating communication networks.

(a) Situation in EB1.
(b) Situation in EB2.
(c) Situation in EB3.
(d) Situation in EB4.

Fig. 14. Simulation results of electricity generation/consumption in plug-and-play case.

(a) Situation in EB1.
(b) Situation in EB2.
(c) Situation in EB3.
(d) Situation in EB4.

Fig. 15. Simulation results of heat generation/consumption in plug-and-play case.

Fig. 16. Energy mismatch in plug-and-play case.

(a) Situation in EB1.
(b) Situation in EB2.
(c) Situation in EB3.
(d) Situation in EB4.

Fig. 17. Simulation results of electricity generation/consumption under varying fixed load.

mismatch in Fig. 16, the energy mismatch fluctuates briefly at 10 s due to the disconnection of the device, but quickly converges to 0. This demonstrates the favorable performance of DNTA in plug-and-play.

In addition we tested the performance of DNTA under time-varying loads. Assuming a scheduling period of 1 h and different values of load in different dispatch periods, the experiments tested the energy production/consumption for 6 dispatch periods. Figs. 17–19 show the production/consumption of electricity, heat and gas for each EB, respectively. It can be seen from the figures that the operation of each intelligent body also changes adaptively due to the change of load. The above experiments clearly show that the DNTA proposed in this paper has good robustness under undesirable factors.

Translated with www.DeepL.com/Translator (free version)

5.3. Contrast performance analysis

In this case study, the DNTA proposed in this paper is compared with the distributed algorithm (DA) proposed in [22] and the distributed recurrent neural network (DRNN) proposed in [23]. To facilitate and visualize the energy generation/consumption profiles of the
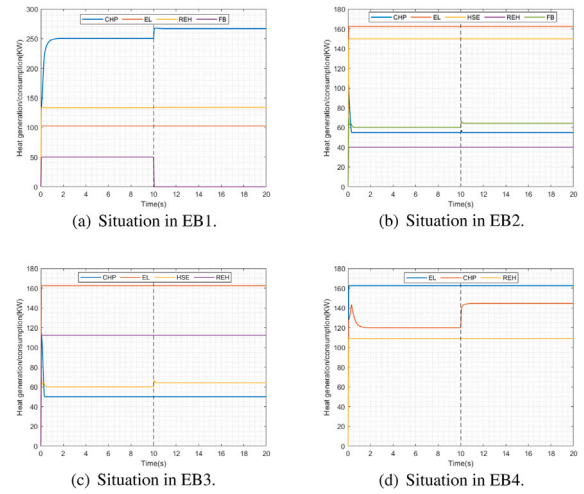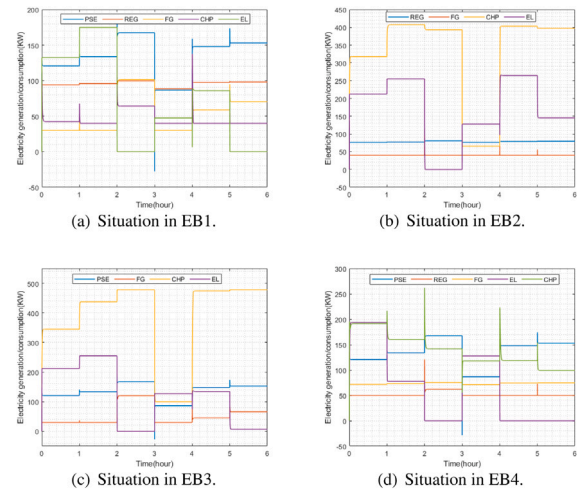
three algorithms, the following average computational accuracy (ACA) is used to measure the convergence speed of the algorithms

$$ACA = \log\left(\frac{\|x - x^*\|_2}{N}\right) \tag{36}$$

where N is the number of variables. Under the same experimental conditions, the experimental results are presented in Fig. 20. The results reveal that DNTA achieves higher accuracy in the same time. This
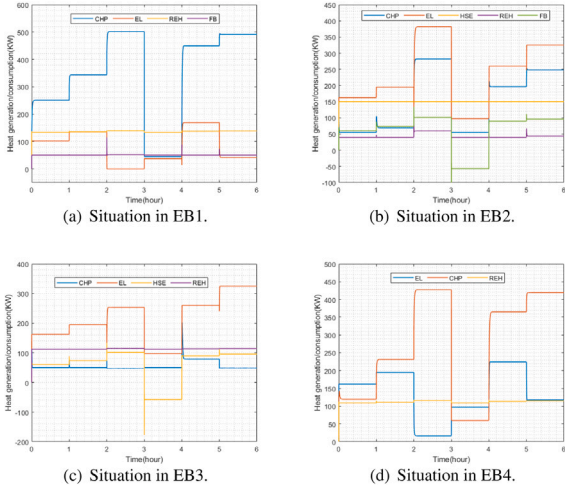
(a) Situation in EB1.

(b) Situation in EB2.

(c) Situation in EB3.

(d) Situation in EB4.

Fig. 18. Simulation results of heat generation/consumption under varying fixed load.
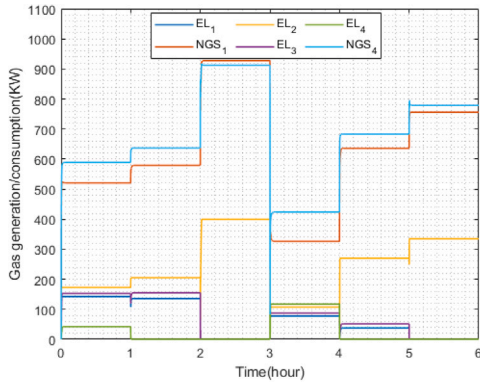

Fig. 19. Simulation results of gas generation/consumption under varying fixed load.

indicates that DNTA achieves optimal operation with faster convergence compared to DA and DRNN. In addition, the energy mismatch of DNTA, DA and DRNN under mutating communication networks is observed on a logarithmic scale to visually demonstrate the advantage of DNTA in terms of robustness. The same setup as in case 2 is used to change the communication connection at $t1 = 20s$ and at $t2 = 40s$. The experimental results are shown in Fig. 21, from which it is clearly observed that the energy mismatch fluctuation of DNTA is smaller at the moment $t1$ and $t2$ when the communication connection is mutated, and DNTA maintains a higher accuracy in the same time. This fully illustrates that the DNTA proposed in this paper has better robustness compared to DA and DRNN.

6. Conclusions

In the context of multi-energy coupling, this paper addresses the EMP in EI scenario for collaborative planning of multiple energy networks. Firstly, the physical structure of EI is introduced, and a distributed energy management model for EI is proposed based on the characteristics of energy supply devices and loads. To address the EMP containing time-varying loads, nonsmooth cost functions and constraints, a DNTA executed in a fully distributed manner is proposed, and a rigorous proof for the optimization and stability of the algorithm is given. Simulation experimental results indicate that the proposed DNTA exhibits favorable stability under communication network mutation, plug-and-play, and time-varying load scenarios. In addition, the DNTA possesses better convergence speed and robustness compared to some
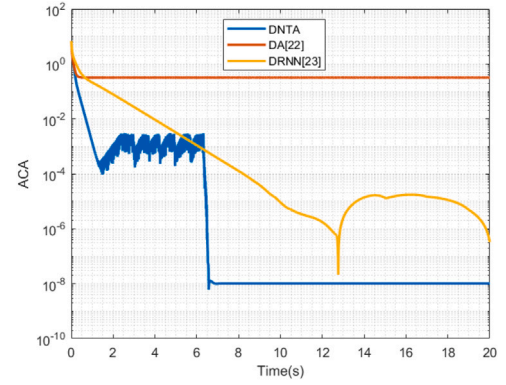

Fig. 20. Results of convergence speed comparison test.

existing works. In future work, energy management of EI in scenarios such as network attacks and delayed communication will be considered to further expand the application scenarios of DNTA.

CRediT authorship contribution statement

Gui Zhao: Conceptualization, Methodology, Writing – original draft, Software, Validation, Visualization, Investigation. **Xing He:** Writing – review & editing. **Guo Chen:** Supervision. **Chaojie Li:** Supervision.

Declaration of competing interest

The authors declare that they have no known competing financial interests or personal relationships that could have appeared to influence the work reported in this paper.

Data availability

The authors do not have permission to share data.

Appendix

The proof of state (*i*): The Lagrange function of the problem (32) is

$$L\left(t, x, \lambda_o, \eta_o\right) = \Phi(x,t) - \lambda_o\left(\tilde{\omega}x - \ell(t)\right) + \eta_o\tilde{\varphi}(x) \tag{A.1}$$

Define x^* is the optimal trajectory of the problem (33), and λ_o^* and η_o^* are the corresponding optimal multipliers, the KKT condition of problem (33) is

$$\partial\Phi(x^*) - \lambda_o^*\tilde{\omega} + \eta_o^*\partial\tilde{\varphi}\left(x^*\right) \in \mathbb{N}_{\tilde{\Omega}}\left(x^*\right) \tag{A.2a}$$

$$\tilde{\omega}x^* = \tilde{\ell}(t) \tag{A.2b}$$

$$\tilde{\varphi}\left(x^*\right) \leqslant 0, \eta_o^* \geqslant 0, \eta_o^*\tilde{\varphi}\left(x^*\right) = 0 \tag{A.2c}$$

Let the optimal trajectory of the DNTA be $\left(\bar{x}, \bar{\lambda}, \bar{y}, \bar{\eta}, \bar{z}\right)$, that is, satisfy

$$\mathbb{0} \in \mathcal{P}_{\tilde{\Omega}}\left(\bar{x} - \partial\Phi(\bar{x}) + \omega^T\bar{\lambda} - \partial\varphi^T(\bar{x})\mathcal{P}_+^{\bar{\eta}}\right) - \bar{x} \tag{A.3a}$$

$$\mathbb{0} = \ell(t) - \omega\bar{x} - \sigma\mathcal{L}\bar{y} \tag{A.3b}$$

$$\mathbb{0} = \sigma\mathcal{L}\bar{\lambda} \tag{A.3c}$$

$$\mathbb{0} \in \mathcal{P}_+^{\bar{\eta}} - \bar{\eta} \tag{A.3d}$$

$$\mathbb{0} = \sigma\mathcal{L}\bar{\eta} \tag{A.3e}$$

For the left multiplication $\left(1_{nm} \otimes I_3\right)$ of formula (A.3b), on the basis of the properties of Laplace matrix and Kronecker product, so that

$$\mathbb{0} = \left(1_{nm} \otimes I_3\right)\left(\ell(t) - \omega\bar{x} - \sigma\mathcal{L}\bar{y}\right) \tag{A.4a}$$

(a) DNTA   (b) DA [22]   (c) DRNN [23]

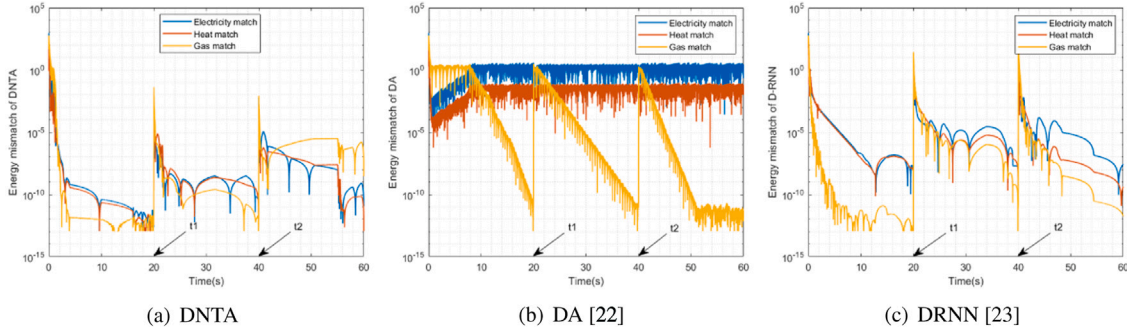**Fig. 21.** Robustness comparison test results.

$$\mathbb{0} = \tilde{\ell}(t) - \tilde{\omega}\bar{x} \tag{A.4b}$$

By complementary relaxation conditions [28], (A.3d) is equivalent to

$$\bar{\eta}^T \left(\tilde{\varphi}(\bar{x}) - \sigma \mathcal{L} \bar{z} \right) = \mathbb{0} \tag{A.5a}$$

$$\bar{\eta} + \tilde{\varphi}(\bar{x}) - \sigma \mathcal{L} \bar{z} \leqslant \mathbb{0} \tag{A.5b}$$

$$\bar{\eta} \geqslant \mathbb{0} \tag{A.5c}$$

Multiply $\left(1_{nm} \otimes I_3 \right)$ on the left of (A.5b) to get $\tilde{\varphi}(\bar{x}) \leqslant \mathbb{0}$. We can get $\forall \bar{\eta}_o$ so that $\bar{\eta} = 1 \otimes \bar{\eta}_o$ holds true according to (A.3e). Furthermore, (A.5a) and (A.5c) are left multiplied by I to obtain

$$\tilde{\varphi}(\bar{x}) \leqslant 0, \bar{\eta}_o \geqslant 0, \bar{\eta}_o \tilde{\varphi}(\bar{x}) = 0$$

From (A.3c)'s point of view, the fact that $\forall \bar{\lambda}$ makes $\bar{\lambda} = 1 \otimes \bar{\lambda}_o$ hold explains

$$\bar{x} - \partial \Phi(\bar{x}) + \omega^T \bar{\lambda} - \partial \varphi^T(\bar{x}) \mathcal{P}_+^{\bar{\eta}}$$
$$= \bar{x} - \partial \Phi(\bar{x}) + \omega^T \left(1 \otimes \bar{\lambda}_o \right) - \partial \varphi^T(\bar{x}) \left(1 \otimes \bar{\eta}_o \right)$$
$$= \bar{x} - \partial \Phi(\bar{x}) + \bar{\lambda}_o \tilde{\omega} - \bar{\eta}_o \partial \tilde{\varphi}(\bar{x}) \tag{A.6}$$

On the basis of the lemma 2.38 of [29], (A.3a) implies $\partial \Phi(\bar{x}) - \bar{\lambda}_o \tilde{\omega} + \bar{\eta}_o \partial \tilde{\varphi}(\bar{x}) \in \mathbb{N}_{\tilde{\Omega}}(\bar{x})$.

In summary, if $\left(\bar{x}, \bar{\lambda}, \bar{y}, \bar{\eta}, \bar{z} \right)$ is the equilibrium trajectory of the DNTA, $\bar{x}$ is the optimal trajectory of the problem (33). Obviously, if x^* is the optimal trajectory of the problem (33), there is an equilibrium trajectory in which $(\lambda^*, y^*, \eta^*, z^*)$ makes $(x^*, \lambda^*, y^*, \eta^*, z^*)$ satisfy the DNTA.

The proof of state (ii): Construct the following candidate Lyapunov function

$$V(t, x, \lambda, y, \eta, z) = V_1(t, x) + V_2(\lambda, y, \eta, z) \tag{A.7}$$

where

$$V_1(t, x) = L\left(t, x, \lambda_o^*, \eta_o^*\right) - L\left(t, x^*, \lambda_o^*, \eta_o^*\right)$$
$$+ \frac{1}{2} \|x - x^*\|^2$$
$$V_2(\lambda, y, \eta, z) = \frac{1}{2} \|\lambda - \lambda^*\|^2 + \frac{1}{2} \|y - y^*\|^2$$
$$+ \frac{1}{2} \|\eta - \eta^*\|^2 + \frac{1}{2} \|z - z^*\|^2$$

Apparently, $V(t, x, \lambda, y, \eta, z)$ is positive definite, local Lipschitz and regularity. $V_1(t, x)$ trajectory along (35) satisfies

$$L_\Gamma V_1 = \left(\partial \Phi(x) - \omega^T \lambda^* + \partial \varphi(x) \eta^* + x - x^* \right)^T \dot{x}$$
$$+ \left(\lambda - \lambda^* \right)^T \omega \dot{x} - \left(\mathcal{P}_+^\eta - \eta^* \right)^T \partial \varphi(x) \dot{x} \tag{A.8}$$

On the basis of Lemma 1, we can get

$$L_\Gamma V_1 \leqslant - \left(x - x^* \right)^T \left(\partial \Phi(x) - \omega^T \lambda + \partial \varphi(x) \mathcal{P}_+^\eta \right)$$
$$- \|\dot{x}\|^2 - \left(\mathcal{P}_+^\eta - \eta^* \right)^T \partial \varphi(x) \dot{x}$$
$$+ \left(\lambda - \lambda^* \right)^T \omega \dot{x}$$

$$= - \left(x - x^* \right)^T \left(\partial \Phi(x^*) - \omega^T \lambda^* + \partial \varphi(x^*) \eta^* \right)$$
$$- \|\dot{x}\|^2 - \left(x - x^* \right)^T \left(\partial \Phi(x) - \partial \Phi(x^*) \right)$$
$$- \left(x - x^* \right)^T \left(\partial \varphi(x) \mathcal{P}_+^\eta - \partial \varphi(x^*) \eta^* \right)$$
$$+ \left(\lambda - \lambda^* \right)^T \omega \dot{x} - \left(\mathcal{P}_+^\eta - \eta^* \right)^T \partial \varphi(x) \dot{x}$$
$$+ \left(x - x^* \right)^T \omega^T \left(\lambda - \lambda^* \right) \tag{A.9}$$

According to the fact that $\Phi(x)$ is a convex function, we can get

$$L_\Gamma V_1 \leqslant - \left(x - x^* \right)^T \left(\partial \varphi(x) \mathcal{P}_+^\eta - \partial \varphi(x^*) \eta^* \right)$$
$$+ \left(x - x^* \right)^T \omega^T \left(\lambda - \lambda^* \right) + \left(\lambda - \lambda^* \right)^T \omega \dot{x}$$
$$- \left(\mathcal{P}_+^\eta - \eta^* \right)^T \partial \varphi(x) \dot{x} \tag{A.10}$$

$V_2(\lambda, y, \eta, z)$ trajectory along (35) satisfies

$$L_\Gamma V_2 = \left(\lambda - \lambda^* \right)^T \dot{\lambda} + \left(y - y^* \right)^T \dot{y} + \left(\eta - \eta^* \right)^T \dot{\eta}$$
$$+ \left(z - z^* \right)^T \dot{z}$$
$$= \left(\lambda - \lambda^* \right)^T \left(\ell(t) - \omega(x + \dot{x}) - \sigma \mathcal{L} \lambda - \sigma \mathcal{L} y \right)$$
$$+ \sigma \left(y - y^* \right)^T \mathcal{L} \lambda + \left(\eta - \eta^* \right)^T \left(\mathcal{P}_+^\eta - \eta \right)$$
$$+ \sigma \left(z - z^* \right)^T \mathcal{L} \mathcal{P}_+^\eta \tag{A.11}$$

In the light of the equilibrium trajectory (A.3) and Lemma 1, we get

$$L_\Gamma V_2 = \left(\lambda - \lambda^* \right)^T \omega \left(x^* - x \right) - \left(\lambda - \lambda^* \right)^T \omega \dot{x}$$
$$- \sigma \lambda^T \mathcal{L} \lambda - \|\dot{\lambda}\|^2 + \left(\mathcal{P}_+^\eta - \eta^* \right)^T \left(\mathcal{P}_+^\eta - \eta \right)$$
$$\leqslant \left(\lambda - \lambda^* \right)^T \omega \left(x^* - x \right) - \left(\lambda - \lambda^* \right)^T \omega \dot{x}$$
$$+ \left(\mathcal{P}_+^\eta - \eta^* \right)^T \varphi(x) - \sigma \left(\mathcal{P}_+^\eta - z^* \right)^T \mathcal{L} \mathcal{P}_+^\eta$$
$$- \sigma \lambda^T \mathcal{L} \lambda + \left(\mathcal{P}_+^\eta - \eta^* \right)^T \partial \varphi(x) \dot{x} \tag{A.12}$$

Thus,

$$L_\Gamma V \leqslant - \left(x - x^* \right)^T \left(\partial \varphi(x) \mathcal{P}_+^\eta - \partial \varphi(x^*) \eta^* \right)$$
$$- \sigma \lambda^T \mathcal{L} \lambda + \left(\mathcal{P}_+^\eta - \eta^* \right)^T \varphi(x)$$
$$- \sigma \left(\mathcal{P}_+^\eta - z^* \right)^T \mathcal{L} \mathcal{P}_+^\eta$$
$$= \left(\varphi(x) - \sigma \mathcal{L} z^* - \left(x - x^* \right)^T \partial \varphi(x) \right)^T \mathcal{P}_+^\eta$$
$$- \left(\varphi(x) - \left(x - x^* \right)^T \partial \varphi(x^*) \right)^T \eta^*$$
$$- \sigma \lambda^T \mathcal{L} \lambda - \sigma \left(\mathcal{P}_+^\eta \right)^T \mathcal{L} \mathcal{P}_+^\eta$$
$$\leqslant \left(\varphi(x) - \varphi(x^*) - \left(x - x^* \right)^T \partial \varphi(x) \right)^T \mathcal{P}_+^\eta$$
$$- \left(\varphi(x) - \varphi(x^*) - \left(x - x^* \right)^T \partial \varphi(x^*) \right)^T \eta^*$$
$$- \sigma \lambda^T \mathcal{L} \lambda - \sigma \left(\mathcal{P}_+^\eta \right)^T \mathcal{L} \mathcal{P}_+^\eta \tag{A.13}$$

By the fact that $\mathcal{L}$ is a positive semidefinite matrix and $\varphi(x)$ is a convex function, it is shown that $L_\Gamma V \leq 0$.

References

[1] M. Roustaee, A. Kazemi, Multi-objective stochastic operation of multi-microgrids constrained to system reliability and clean energy based on energy management system, Electr. Power Syst. Res. 194 (2021) 106970.

[2] A.G. Daryan, A. Sheikhi, A.A. Zadeh, Peer-to-Peer energy sharing among smart energy hubs in an integrated heat-electricity network, Electr. Power Syst. Res. 206 (2022) 107726.

[3] C. Li, N. Wang, Z. Wang, X. Dou, Y. Zhang, Z. Yang, F. Maréchal, L. Wang, Y. Yang, Energy hub-based optimal planning framework for user-level integrated energy systems: Considering synergistic effects under multiple uncertainties, Appl. Energy 307 (2022) 118099.

[4] B. Liu, Y. Peng, J. Xu, C. Mao, D. Wang, Q. Duan, Design and implementation of multiport energy routers toward future energy internet, IEEE Trans. Ind. Appl. 57 (3) (2021) 1945–1957.

[5] J. Zhang, Distributed network security framework of energy internet based on internet of things, Sustain. Energy Technol. Assess. 44 (2021) 101051.

[6] Y. Li, D.W. Gao, W. Gao, H. Zhang, J. Zhou, A distributed double-Newton descent algorithm for cooperative energy management of multiple energy bodies in energy internet, IEEE Trans. Ind. Inf. 17 (9) (2021) 5993–6003.

[7] A.R.D. Fazio, C. Risi, M. Russo, M.D. Santis, Coordinated optimization for zone-based voltage control in distribution grids, IEEE Trans. Ind. Appl. 58 (1) (2022) 173–184.

[8] A.R.D. Fazio, C. Risi, M. Russo, M.D. Santis, Decentralized voltage optimization based on the auxiliary problem principle in distribution networks with DERs, Appl. Sci. 11 (10) (2021) 4509.

[9] T. Hong, Y. Zhang, Data-driven optimization framework for voltage regulation in distribution systems, IEEE Trans. Power Deliv. 37 (2) (2022) 1344–1347.

[10] S. Sharma, A. Verma, B.K. Panigrahi, Robustly coordinated distributed voltage control through residential demand response under multiple uncertainties, IEEE Trans. Ind. Appl. 57 (4) (2021) 4042–4058.

[11] Y. Chai, L. Guo, C. Wang, Y. Liu, Z. Zhao, Hierarchical distributed voltage optimization method for HV and MV distribution networks, IEEE Trans. Smart Grid 11 (2) (2020) 968–980.

[12] L. Yin, Y. Lu, Expandable quantum deep width learning-based distributed voltage control for smart grids with high penetration of distributed energy resources, Int. J. Electr. Power Energy Syst. 137 (2022) 107861.

[13] Z. Yi, Y. Xu, J. Hu, M.-Y. Chow, H. Sun, Distributed, neurodynamic-based approach for economic dispatch in an integrated energy system, IEEE Trans. Ind. Inf. 16 (4) (2020) 2245–2257.

[14] P. Feng, X. He, Mixed neurodynamic optimization for the operation of multiple energy systems considering economic and environmental aspects, Energy 232 (2021) 120965.

[15] X. He, Y. Zhao, T. Huang, Optimizing the dynamic economic dispatch problem by the distributed consensus-based ADMM approach, IEEE Trans. Ind. Inf. 16 (5) (2020) 3210–3221.

[16] D. Li, L. Yu, N. Li, F. Lewis, Virtual-action-based coordinated reinforcement learning for distributed economic dispatch, IEEE Trans. Power Syst. 36 (6) (2021) 5143–5152.

[17] C. Zhao, X. Duan, Y. Shi, Analysis of consensus-based economic dispatch algorithm under time delays, IEEE Trans. Syst. Man Cybern.: Syst. 50 (8) (2020) 2978–2988.

[18] P. Dai, W. Yu, G. Wen, S. Baldi, Distributed reinforcement learning algorithm for dynamic economic dispatch with unknown generation cost functions, IEEE Trans. Ind. Inf. 16 (4) (2020) 2258–2267.

[19] Y. Zhu, W. Ren, W. Yu, G. Wen, Distributed resource allocation over directed graphs via continuous-time algorithms, IEEE Trans. Syst. Man Cybern.: Syst. 51 (2) (2021) 1097–1106.

[20] H. Zhang, Y. Li, D.W. Gao, J. Zhou, Distributed optimal energy management for energy internet, IEEE Trans. Ind. Inf. 13 (6) (2017) 3081–3097.

[21] Q. Li, Y. Liao, K. Wu, L. Zhang, J. Lin, M. Chen, J.M. Guerrero, D. Abbott, Parallel and distributed optimization method with constraint decomposition for energy management of microgrids, IEEE Trans. Smart Grid 12 (6) (2021) 4627–4640.

[22] S. Liang, X. Zeng, G. Chen, Y. Hong, Distributed sub-optimal resource allocation via a projected form of singular perturbation, Automatica 121 (2020) 109180.

[23] X. Le, S. Chen, F. Li, Z. Yan, J. Xi, Distributed neurodynamic optimization for energy internet management, IEEE Trans. Syst. Man Cybern.: Syst. 49 (8) (2019) 1624–1633.

[24] Y. Zhao, X. Liao, X. He, R. Tang, Centralized and collective neurodynamic optimization approaches for sparse signal reconstruction via L1-minimization, IEEE Trans. Neural Netw. Learn. Syst. (2021).

[25] X. Zeng, P. Yi, Y. Hong, L. Xie, Continuous-time distributed algorithms for extended monotropic optimization problems, SIAM J. Control Optim. 56 (6) (2016) 3973–3993.

[26] J. Cortes, Discontinuous dynamical systems, IEEE Control Syst. Mag. 28 (3) (2008) 36–73.

[27] X. Chang, Y. Xu, W. Gu, H. Sun, M.-Y. Chow, Z. Yi, Accelerated distributed hybrid stochastic/robust energy management of smart grids, IEEE Trans. Ind. Inf. 17 (8) (2021) 5335–5347.

[28] P. Li, Y. Zhao, J. Hu, Y. Zhang, B.K. Ghosh, Distributed initialization-free algorithms for multi-agent optimization problems with coupled inequality constraints, Neurocomputing 407 (2020) 155–162.

[29] A. Ruszczynski, Nonlinear Optimization, Princeton University Press, 2011.